Coupling of a surface plasmon with localized subwavelength microcavity modes

P. Jouy,[1] Y. Todorov,[1,a)] A. Vasanelli,[1] R. Colombelli,[2] I. Sagnes,[3] and C. Sirtori[1]
[1]*Laboratoire "Matériaux et Phénomènes Quantiques," Université Paris Diderot-Paris 7, CNRS-UMR 7162, 75013 Paris, France*
[2]*Institut d'Electronique Fondamentale, Univ. Paris-Sud, UMR8622 CNRS, 91405 Orsay, France*
[3]*CNRS/Laboratoire de Photonique et de Nanostructures (LPN), Route de Nozay, 91460 Marcoussis, France*

(Received 19 November 2010; accepted 20 December 2010; published online 11 January 2011)

Midinfrared photonic modes of a periodically patterned metal-dielectric-metal structure have been investigated theoretically and experimentally. We have observed an anticrossing behavior between cavity modes localized in the double-metal regions and the surface plasmon polariton, signature of a hybridization between the two modes. © *2011 American Institute of Physics*.
[doi:10.1063/1.3536504]

A metal-dielectric interface supports the well known surface plasmon-polariton (SPP) modes, yielded by the coupling of the electromagnetic field with the coherent oscillations of the free electrons in the metal.[1,2] Their ability to store and propagate the electromagnetic energy at subwavelength scales is essential for many applications such as biosensing, photonic circuits, and optical data storage.[3–5] However, the plasmon-polariton decay length in the air, δ, strongly increases with the wavelength λ, compromising the subwavelength energy confinement in the midinfrared (mid-IR) and terahertz part of the spectrum.[6] Recently, the concept of "spoof" surface plasmons has been put forward,[7] where shorter decay lengths can be engineered by drilling subwavelength holes in a thick metal substrate. An older but efficient method of localizing the SPP near the surface is coating the metal with a thin high refractive index dielectric material.[8] In this letter we report on structures where a metallic strip grating is deposited on a GaAs-coated metal. This structure supports modes which are localized between the two metals[9,10] and yet able to efficiently couple with the surface plasmon guided by the air-semiconductor-metal multilayer. This coupling effect occurs for well defined choices of the grating periodicity and GaAs thickness and allows us to control the properties of the free propagating surface waves.

In our experimental structure a 300 nm thick undoped semiconductor (gallium arsenide) slab is sandwiched between two golden parts, one of which is patterned as a rectangular strip grating of width s and period p, as illustrated in Fig. 1(a). The typical dimensions of the structure, which have been fabricated by e-beam lithography, are $s=0.4–3.5$ μm and $p=1.5–4.8$ μm. The thickness of the grating strips is 87 nm. Similar structures, but with micrometric dimensions, are known to support electromagnetic modes which are strongly localized under the grating strips in the microwave and terahertz regions.[9,10] These modes originate from the TM_0 mode confined in the double-metal regions.[10] The multiple reflections of the TM_0 mode between the two ends of the metal strips yield standing wave patterns, as illustrated in Fig. 1(b). The resonant wavelengths λ_K are provided by the formula

$$\lambda_K = 2n_M(\lambda_K)s/K. \quad (1)$$

Here K is a nonzero integer, corresponding to the number of nodes of the vertical electric field E_z and n_M is an effective index which depends on the metal losses and the impedance mismatch on the resonator ends.[10] This quantity is wavelength dependent $n_M=n_M(\lambda)$, varying monotonically between 4.5 and 6.6 in the explored wavelength range ($\lambda=5–15$ μm). As expected, these values are higher than the refractive index of the semiconductor, $n_{GaAs}=3.3$.[10]

The structures are analyzed by performing reflectivity spectra, where the cavity modes appear as Lorentzian dips of typical full width at half maximum of 25 meV. The corresponding typical quality factors are $Q\sim6$, lower than the values $Q\sim10$ observed in the far-infrared region[10] due to the

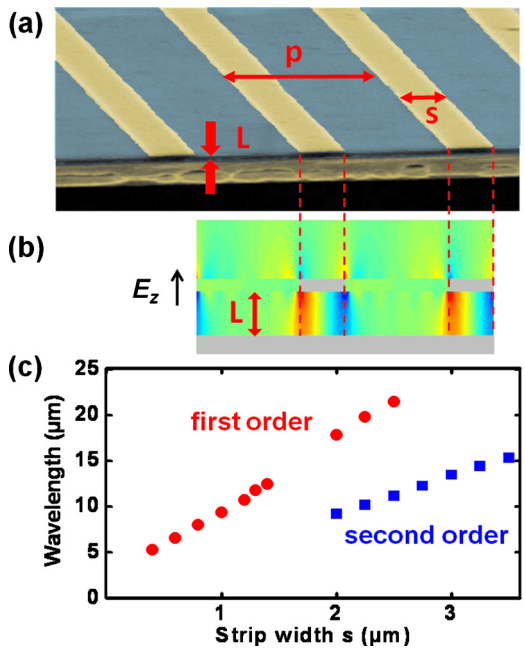

FIG. 1. (Color online) (a) Scanning electron microscope picture of the device in false colors, with the relevant geometrical parameters. (b) Simulation of the vertical electric field (E_z) distribution for the lowest order cavity mode. (c) Resonant wavelengths for the first order (dots) and second order (squares) as a function of the strip width s, determined from reflectivity measurements.

a)Electronic mail: yanko.todorov@univ-paris-diderot.fr.

 © 2011 American Institute of Physics

Downloaded 13 Jan 2011 to 129.175.97.14. Redistribution subject to AIP license or copyright; see http://apl.aip.org/about/rights_and_permissions

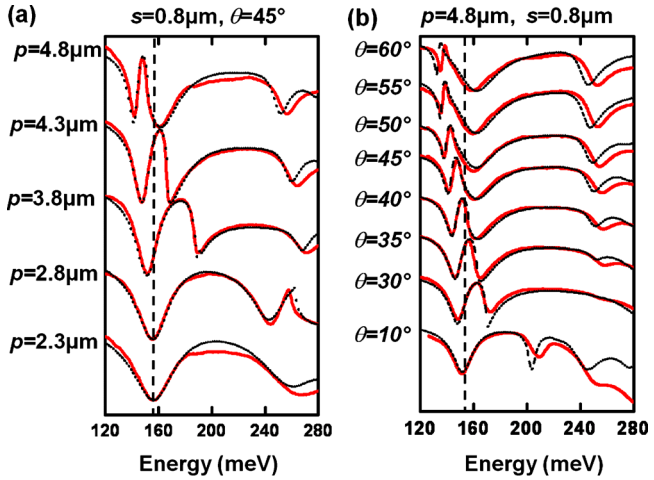

FIG. 2. (Color online) (a) Experimental reflectivity spectra (continuous lines) for structures with strip width $s=0.8\ \mu$m and variable grating period p. The incident angle is $\theta=45°$. (b) Reflectivity spectra (continuous lines) for a structure with strip width $s=0.8\ \mu$m and period $p=4.8\ \mu$m for different incident angles θ. In both (a) and (b) we provide simulated spectra in (black) dotted curves. The dashed line indicates the bare cavity resonance.

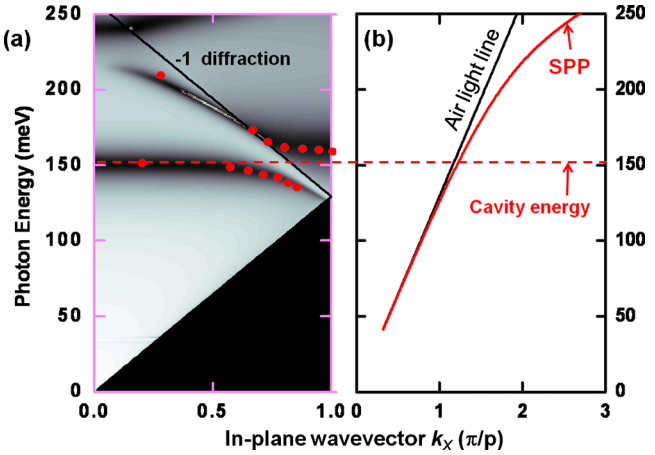

FIG. 3. (Color online) (a) Simulated reflectivity as a function of the photon energy E and wave vector k_x for the first Brillouin zone of the grating with $p=4.8\ \mu$m, together with the experimental peak positions from Fig. 2(b) (dots). (b) Dispersion relation of the GaAs-coated metal planar surface plasmon. The wave vector k_x has been normalized to the grating wave vector π/p ($p=4.8\ \mu$m) for comparison with (a). The dashed line indicates the bare cavity resonance.

increased metal losses at shorter wavelengths. Figure 1(c) summarizes the experimentally measured resonant wavelengths of the first ($K=1$) and the second ($K=2$) orders for an incident angle $\theta=45°$. The measured effective index is $n_M \sim 4.6$ for the first order ($K=1$) resonance, around 150 meV. For these structures the grating period is kept low, $p<3\ \mu$m, and it remains essentially smaller than the wavelength, as in Ref. 10. For these periods the cavity resonances are below the onset of diffraction, and they do not feature any dispersion as a function of the incident wave vector $k_x=(\omega/c)\sin\theta$.

However, the situation changes completely when the period p is comparable to $\lambda/2$. In this case the diffraction phenomena interfere with the localized modes and modify their line shape and dispersion relation. The first diffraction order to come into play is the -1 diffracted order, which appears for a wavelength λ_{-1},

$$\lambda_{-1}=p(1+\sin\theta). \tag{2}$$

This is illustrated in the data set presented in Figs. 2(a) and 2(b) in continuous curves. For all samples, the strip width is $s=0.8\ \mu$m, which sets the energy of the fundamental cavity mode ($K=1$) at 151 meV ($\lambda_{K=1}=8.2\ \mu$m). We have then let vary either the angle of incidence θ or the grating period p in order to tune the diffraction edge [Eq. (2)] across the cavity resonance. In Fig. 2(a), the incident angle is fixed, $\theta=45°$, and the reflectivity is studied for progressively increasing grating periods p. We observe that when $\lambda_{K=1}=\lambda_{-1}$ the cavity mode splits in two. Similar behavior is observed from the data reported in Fig. 2(b) where the period is fixed, $p=4.8\ \mu$m, but the incident angle θ is varied. For low angles we recover the "bare" cavity mode at 151 meV, and the cavity mode splits in two for large incident angles when $\lambda_{K=1}=\lambda_{-1}$.

The experimental reflectivity spectra of Figs. 2(a) and 2(b) are very well reproduced by our simulations, indicated by (black) dotted curves, based on the modal method formalism with surface impedance boundary conditions.[11] The input parameter for the model is the gold dielectric constant, for which we use a Drude-like susceptibility $\varepsilon(E)=1-2.29\times10^7/[E(E+i145)]$, where E is the photon energy in meV. Note that the metal losses in this formula are increased with respect to the bulk values known from the literature,[12] possibly due to scattering on the semiconductor-metal interface and the presence of thin (6 nm) Ti adhesive layers between the semiconductor and the gold coatings.

The effect of the diffraction edge on the cavity resonance is best illustrated in Fig. 3(a) where we plot the simulated reflectivity as a function of the photon energy E and incident wave vector k_x for the first Brillouin zone of the grating with $p=4.8\ \mu$m, together with the experimental peak positions from Fig. 2(b) (dots). This diagram shows that the cavity mode at 151 meV is indeed dispersionless far from the diffraction limit, whereas a clear anticrossing behavior is observed close to the -1 diffraction line. This anticrossing appears because of the coupling between the cavity mode and the SPP supported by the air-semiconductor-metal multilayer, excited in the vicinity of λ_{-1}.[2] Note that, away from the anticrossing region, our structure acts like a leaky wave antenna for the SPP guided in the multilayer.[13] The dispersion relation of this SPP is plotted in Fig. 3(b) for the case of planar GaAs-coated metal surface without any grating. For the sake of comparison with Fig. 3(a) the wave vector is still normalized to π/p and the energy of the bare cavity mode is indicated with a dashed line. From this diagram, we deduce an anticrossing wave vector $k_x=1.22\pi/p$, which corresponds to a $(2-1.22)\pi/p=0.78\pi/p$ in the first Brillouin zone of the grating, in accordance with the experimental results reported in Fig. 3(a).

The dispersion relation of the GaAs-coated plasmon in Fig. 3(b) gives a hint on the coupling mechanism. Indeed, for midinfrared frequencies, the simple air-metal surface plasmon follows tightly the light line, whereas the 300 nm GaAs-coated plasmon is increasingly pulled below the air light line for higher energies (shorter wavelengths). The SPP decay length in the air can be simply expressed as $\delta=1/\sqrt{k_x^2-\omega^2/c^2}$ and therefore for higher photon energies, while δ decreases the SPP has a stronger overlap with the semiconductor region, favoring the interaction with the strongly localized cavity modes. This is indeed the case as

Downloaded 13 Jan 2011 to 129.175.97.14. Redistribution subject to AIP license or copyright; see http://apl.aip.org/about/rights_and_permissions

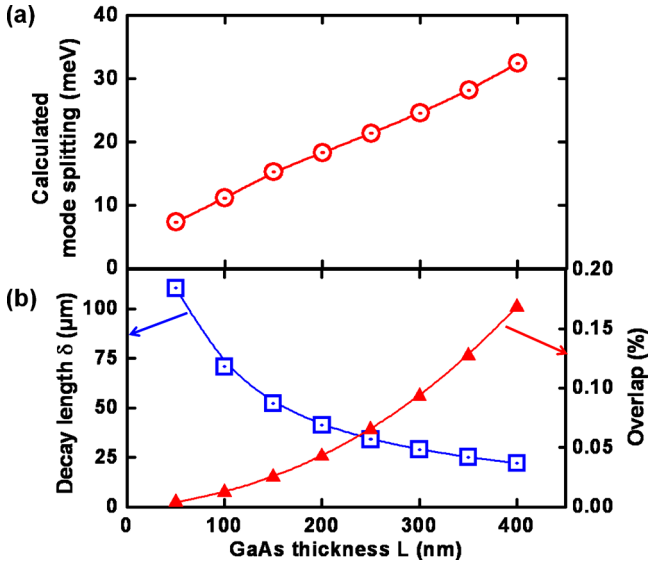

FIG. 4. (Color online) (a) Mode splitting at the anticrossing point as a function of the GaAs thickness L, computed for a structure with $p=4.8$ μm and $s=0.6$ μm. For these simulations, the anticrossing appears for a wave vector $k_x=0.5\pi/p$. (b) Decay length (open squares) and vertical electric field (E_z) overlap with the semiconductor layer (triangles) for a planar surface plasmon as a function of the GaAs thickness L.

illustrated in Fig. 4(a), which resumes the simulated mode splitting as a function of the coating thickness L. For these simulations, the grating period is $p=4.8$ μm, and for convenience the metal strip width is chosen to be $s=0.6$ μm (cavity resonance at $\lambda_{K=1}=6.6$ μm), so that the anticrossing appears in the middle of the first Brillouin zone of the grating at $k=0.5\pi/p$. In Fig. 4(b) we have plotted δ (open squares) of the planar GaAs-coated surface plasmon as well as the electric field overlap with the semiconductor region (triangles) as a function of L for the wave vector corresponding to the anticrossing point. As expected, for increasing thickness the overlap of the plasmon field with the semiconductor also increases and δ decreases. Note that even subwavelength coatings ($L=400$ nm) are sufficient to reduce significantly the plasmon decay length in the air: from 120 to 20 μm.

The strong interaction between the surface plasmon and the cavity modes means a periodic exchange of the electromagnetic energy between the two. As shown in Ref. 10 the cavity modes have the ability to convert and store very efficiently the energy of the incoming wave into evanescent near field. Therefore, thanks to the coupling mechanism evidenced above, the cavity modes mediate the energy transfer between the radiation modes and the evanescent surface plasmon mode, allowing the excitation of the SPP with an increased efficiency. The interference between the two coupled modes with the evanescent background of the grating also explains the distorted Fano-like line shapes observed in the spectra of Figs. 2(a) and 2(b) close to the diffraction line, as pointed out by Sarrazin *et al.*[14]

In conclusion, we have experimentally demonstrated strongly localized cavity modes supported by compact metal-semiconductor-metal grating structures scaled to operate at the mid-IR frequency range. We have observed the strong coupling between these modes and the surface plasmon also supported by the air-dielectric-metal structure. The latter has an increased confinement of the electromagnetic energy above the metal-air interface. Since for this frequency range the semiconductor can be engineered into a quantum cascade gain medium, this opens a variety of perspectives for electrical generation or amplification[15] of surface plasmons and the building of very compact SPP circuits in the mid-IR frequency range.

We thank Michael Rosticher (Ecole Nomale Supérieure, Paris) for help with the e-beam lithography system. This work has been partially supported by the French National Research Agency (ANR) in the frame of its Nanotechnology and Nanosystems program P2N, Project No. ANR-09-NANO-007. Part of the device fabrication has been performed at the CTU-IEF-Minerve which was partially funded by the "Conseil Général de l'Essonne."

[1] R. H. Ritchie, Phys. Rev. **106**, 874 (1957).
[2] H. Raether, *Surface Plasmons on Smooth and Rough Surfaces and on Gratings* (Springer, Berlin, 1988).
[3] W. L. Barnes, A. Dereux, and T. W. Ebbesen, Nature (London) **424**, 824 (2003).
[4] S. Lal, S. Link, and N. J. Halas, Nat. Photonics **1**, 641 (2007).
[5] T. W. Ebbesen, C. Genet, and S. Bozhevolnyi, Phys. Today **61**(5), 44 (2008).
[6] W. L. Barnes, J. Opt. A, Pure Appl. Opt. **8**, S87 (2006).
[7] J. B. Pendry, L. Martin-Moreno, and F. J. Garcia-Vidal, Science **305**, 847 (2004).
[8] I. Pockrand, Surf. Sci. **72**, 577 (1978).
[9] A. P. Hibbins, J. R. Sambles, C. R. Lawrence, and J. R. Brown, Phys. Rev. Lett. **92**, 143904 (2004).
[10] Y. Todorov, L. Tosetto, J. Teissier, A. M. Andrews, P. Klang, R. Colombelli, I. Sagnes, G. Strasser, and C. Sirtori, Opt. Express **18**, 13886 (2010).
[11] Y. Todorov and C. Minot, J. Opt. Soc. Am. A **24**, 3100 (2007).
[12] *Handbook of Optical Constants of Solids*, edited by E. Palik (Academic Press, San Diego, 1998).
[13] A. A. Oliner and D. R. Jackson, in *Antenna Engineering Handbook*, edited by J. L. Volakis (McGraw-Hill, New York, 2007), Chap. 11.
[14] M. Sarrazin, J. P. Vigneron, and J. M. Vigoureux, Phys. Rev. B **67**, 085415 (2003).
[15] A. Babuty, A. Bousseksou, J.-P. Tetienne, I. Doyen, C. Sirtori, G. Beaudoin, I. Sagnes, Y. De Wilde, and R. Colombelli, Phys. Rev. Lett. **104**, 226806 (2010).

Downloaded 13 Jan 2011 to 129.175.97.14. Redistribution subject to AIP license or copyright; see http://apl.aip.org/about/rights_and_permissions